An *LC*-Compensated Electric Field Repeater for Long-Distance Capacitive Power Transfer

Hua Zhang, *Student Member, IEEE*, Fei Lu, *Student Member, IEEE*, Heath Hofmann, *Senior Member, IEEE*, Weiguo Liu, *Senior Member, IEEE*, and Chunting Chris Mi, *Fellow, IEEE*

***Abstract*—This paper proposes an *LC*-compensated electric field repeater to extend the transfer distance of a capacitive power transfer (CPT) system. The repeater contains two metal plates connected with an external capacitor and an external inductor. The plates are used to generate electric fields to transfer power. The external inductor and capacitor are used to resonate with the plates in order to increase the voltage levels. The repeater is placed between a transmitter and a receiver, which also contains metal plates compensated by an *LC* network. The repeater can increase the transfer distance of the CPT system without significantly influencing the system power and efficiency. In this paper, the capacitive coupler structure and dimensions are designed and simulated using Maxwell software. Considering all the capacitive coupling between plates, an equivalent circuit model is derived. The fundamental harmonics approximation method is used to analyze the working principle of the circuit. A 150 W input power CPT system is designed as an example to validate the proposed repeater structure and compensation circuit topology. The system can achieve an efficiency of 66.9% from dc source to dc load, when the transfer distance is 360 mm and the repeater is placed between the transmitter and the receiver.**

***Index Terms*—Capacitive power transfer (CPT), electric fields, *LC* compensation, long-distance power transfer, power repeater, wireless power transfer (WPT).**

I. Introduction

WIRELESS power transfer (WPT) is an effective and convenient method to deliver power without direct metal-to-metal contact. Present WPT technologies includes inductive power transfer (IPT) and capacitive power transfer (CPT). The IPT system has been widely studied and used, in which magnetic fields are used to transfer power [1]–[4]. It has been applied in contactless slip-ring of motor [5], mobile devices charging [6], and high-power electric vehicles, and the efficiency can be higher than 95% [7], [8]. However, the high-frequency magnetic fields can induce eddy current losses in metal materials nearby, which limit its application area.

The CPT system is an alternative option to overcome the above drawbacks. It utilizes electric fields to transfer power, which can encounter metal objects without generating significant power losses. Also, it uses metal plates to replace the expensive Litz-wire typically used in an IPT coupler, which can reduce the system cost [9].

The challenge in CPT comes from the conflict between the transfer distance and the capacitance value. When the distance increases to hundreds of millimeters range, the coupling capacitance is usually in the several pF range, which is difficult to transfer high power. Therefore, some references focus on short distance ($<$1.0 mm) applications, where the coupling capacitance can reach up to tens of nF [10]–[12]. Some others propose to increase the switching frequency to the tens of MHz. However, the system efficiency is then limited by the high-frequency power amplifier [13]–[15].

An *LCLC* compensation network was proposed in [16] and [17], which can achieve 2.4 kW power transfer over an air-gap distance of 150 mm. An issue of this topology is that it requires eight circuit components in the compensation network. The coupler structure can be optimized to improve the misalignment ability [18]. The CPT system can also be combined with an IPT system to increase the total power [19].

In some applications, the transfer distance needs to be significantly increased. This can be accomplished with a power repeater [20]–[22]. It has been demonstrated in an IPT system, the power transfer direction can also be controlled through the repeater position.

In this paper, an *LC*-compensated electric field repeater is proposed to extend the power transfer distance of a CPT system [23]. Compared with [23], this paper is significantly expanded and there are three improvements. First, Section II provides the full-capacitor model and equivalent behavior source model of the repeater coupler, which allows a better understanding of the repeater system. Second, the analysis of the circuit working principle in Section III is improved to provide a more accurate calculation of system power. Third, more simulation

Manuscript received September 23, 2016; revised December 25, 2016 and February 28, 2017; accepted April 19, 2017. Date of publication April 25, 2017; date of current version September 18, 2017. Paper 2016-TSC-1015.R2, presented at the 2016 IEEE Energy Conversion Congress and Exposition, Milwaukee, WI USA, Sep. 18–22, and approved for publication in the IEEE TRANSACTIONS ON INDUSTRY APPLICATIONS by the Transportation Systems Committee of the IEEE Industry Applications Society. *(Corresponding author: Chunting Chris Mi).*

H. Zhang is with Northwestern Polytechnical University, Xi'an 710072, China, and also with San Diego State University, San Diego, CA 92182 USA (e-mail: hzhang@mail.sdsu.edu).

F. Lu is with San Diego State University, San Diego, CA 92182 USA, and also with the University of Michigan–Ann Arbor, Ann Arbor, MI 48109 USA (e-mail: feilu@umich.edu).

H. Hofmann is with the University of Michigan–Ann Arbor, Ann Arbor, MI 48109 USA (e-mail: hofmann@umich.edu).

W. Liu is with Northwestern Polytechnical University, Xi'an 710072, China (e-mail: lwglll@nwpu.edu.cn).

C. C. Mi is with San Diego State University, San Diego, CA 92182 USA (e-mail: mi@ieee.org).

Color versions of one or more of the figures in this paper are available online at http://ieeexplore.ieee.org.

Digital Object Identifier 10.1109/TIA.2017.2697846

and experimental results are provided in Sections IV and V. There are more design details of the prototype and discussions of the experimental results, such as the power and efficiency relationship, the power loss distribution, the repeater position variation. Finally, results are compared with nonrepeater systems.

The *LC* circuit is a simplification of the *LCLC* topology [16], and fewer components are used for easy implementation. This topology and the concept of the electric field repeater are also mentioned in [24]. However, this paper has three differences and improvements compared to [24].

First, the compensation circuit topology in this paper is different. Previously, parasitic capacitances between adjacent plates on the same side are used as the self-capacitances, and there is no external capacitor connected to the coupler. Therefore, it is strictly a simple series-compensated topology, and the switching frequency is as high as 27.12 MHz due to the extremely small capacitance. However, the proposed system in this paper contains external capacitors connected to the coupler to increase the self-capacitances. The switching frequency is reduced to 1.5 MHz, which is feasible for more semiconductor devices.

Second, this paper provides the solution from dc-source to dc load. In previous references, since the switching frequency is high, a power amplifier is usually required to supply ac excitation to the resonant circuit, and the system efficiency measurement does not include the power amplifier. However, the efficiency of the power amplifier is usually very low and its volume is very large, which limits the applications of CPT technology. In this paper, since the frequency is lower, a simple full-bridge inverter working at soft-switching condition can be used to realize the CPT system.

Third, this paper provides the detailed circuit working principle and design process of the electric field repeater system. Three pairs of metal plates are used as the power transmitter, repeater, and receiver, respectively. For each pair of plates, an external inductor and an external capacitor are connected in parallel to provide resonance and thus achieve high voltages. A 150 W input power CPT system switching at 1.5 MHz is implemented to validate the CPT repeater. All circuit parameter values are provided. The circuit working principle is validated by both simulations and experiments. The experimental results show that the transfer distance is doubled from 180 to 360 mm with the repeater, and the dc–dc efficiency is 66.9%.

II. Capacitive Coupler Design

A. Coupler Structure

Aluminum plates are used to realize the capacitive coupler. The structure and dimensions of the capacitive coupler are presented in Fig. 1. P_1 and P_2 work as the transmitter, P_3 and P_4 are the repeater plates, and P_5 and P_6 work as the receiver. To simplify the design process, the shape of the plates is square. In practical applications, the plate shape can vary, but the total area has to be maintained to achieve large enough coupling capacitances.

In this design, the plate size is defined as l_1. The plate separation on the same side is defined as d_1. The air-gap distance between the transmitter and repeater is defined as d_2, and the air-gap distance between the repeater and receiver is defined as d_3. The distance d_1 relates to the self-coupling at each side, and the distances d_2 and d_3 relate to the mutual couplings between different sides.

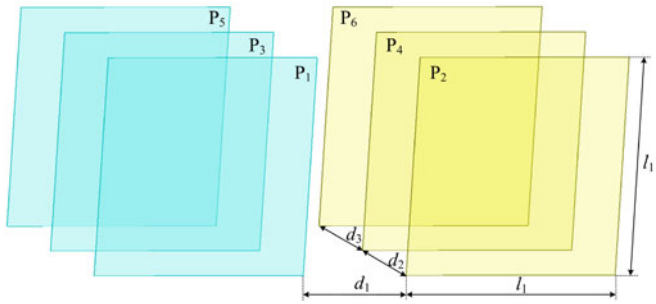

Fig. 1. Structure and dimensions of the capacitive coupler.

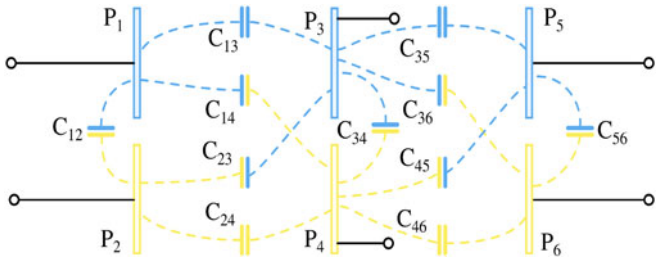

Fig. 2. Capacitances between each pair of plates.

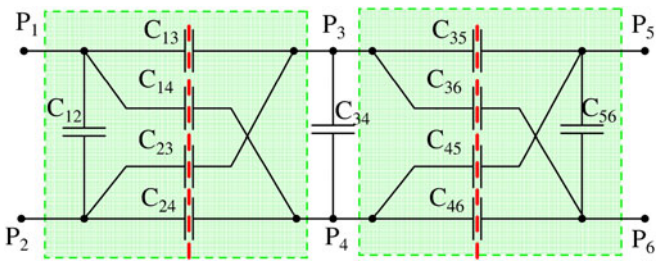

Fig. 3. Full-capacitor model of the capacitive coupler.

B. Equivalent Circuit Model

Fig. 2 shows the capacitances between each pair of plates. All capacitances between adjacent plates are considered. Since the transmitter and receiver are placed far from each other and are separated by the repeater, the four capacitances between them (C_{15}, C_{16}, C_{25}, and C_{26}) are neglected to simplify the circuit analysis.

Fig. 3 shows the full-capacitor model of the capacitive coupler. There are in total 11 capacitors considered in this design. Considering the equivalent circuit model of the four-plate coupler in [18], the full-capacitor model can be separated into two parts, as shown in Fig. 3. The equivalent models of the left and right parts can be derived separately using Kirchhoff's Current Law (KCL) equations as shown in [18]. Therefore, the equivalent behavior source model and π model of the capacitive coupler with a repeater are shown in Figs. 4 and 5, respectively. The relationships between the parameters are further shown in

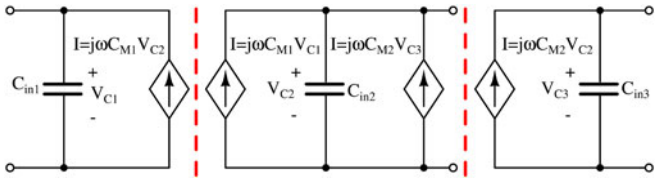

Fig. 4. Behavior source model of the capacitive coupler.

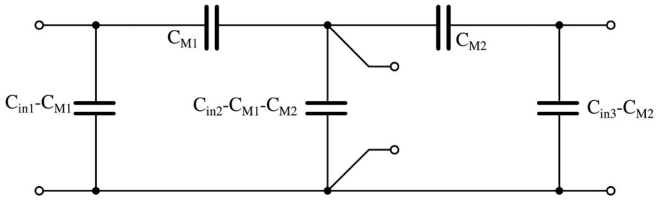

Fig. 5. Equivalent π model of the capacitive coupler.

the following equation:

$$\begin{cases} C_{\text{in}1} = C_{12} + \dfrac{(C_{13}+C_{14})\cdot(C_{23}+C_{24})}{C_{13}+C_{14}+C_{23}+C_{24}} \\ C_{\text{in}2} = C_{34} + \dfrac{(C_{13}+C_{23})\cdot(C_{14}+C_{24})}{C_{13}+C_{14}+C_{23}+C_{24}} \\ \qquad + \dfrac{(C_{35}+C_{45})\cdot(C_{36}+C_{46})}{C_{35}+C_{45}+C_{36}+C_{46}} \\ C_{\text{in}3} = C_{56} + \dfrac{(C_{35}+C_{36})\cdot(C_{45}+C_{46})}{C_{35}+C_{45}+C_{36}+C_{46}} \\ C_{M1} = \dfrac{C_{24}C_{13}-C_{14}C_{23}}{C_{13}+C_{14}+C_{23}+C_{24}} \\ C_{M2} = \dfrac{C_{46}C_{35}-C_{45}C_{36}}{C_{35}+C_{45}+C_{36}+C_{46}} \end{cases} . \quad (1)$$

According to the behavior source model in Fig. 4, the capacitances $C_{\text{in}1}$, $C_{\text{in}2}$, and $C_{\text{in}3}$ represent the capacitances at the same port, and so are defined as self-capacitances. The capacitances C_{M1} and C_{M2} represent the interaction with other ports, and so are defined as mutual capacitances.

C. Maxwell Simulation

Maxwell software can be used to simulate the electric field distribution and the coupling capacitances for different dimensions. The simulation results can provide the coupling capacitances between each pair of plates as shown in Fig. 2. Then, (1) is used to determine the equivalent capacitances.

The metal plates are chosen to be square and identical to simplify the dimension design process. The plate geometry is selected according to the aluminum plates available in the lab. The plate length l_1 is set to be 300 mm. Also, considering the fixture size available in the lab, the plate distance d_1 is 150 mm. The total air-gap distance is fixed to $d_2 + d_3 = 360$ mm as a design example. Maxwell three-dimensional simulations are used to find the relationship between d_2 and the coupling capacitances.

Fig. 6 shows the Maxwell simulation results of the mutual capacitance over a range of d_2 values. It shows that C_{M1} decreases with increasing d_2, and C_{M2} increases with increasing d_2. Fig. 7 shows the simulation results of the self-capacitance over a range of d_2 values. When the repeater is in the middle of the transmitter and receiver ($d_2 = 180$ mm), $C_{M1} = C_{M2} = 2.8$ pF, $C_{\text{in}1} = C_{\text{in}3} = 8.1$ pF, and $C_{\text{in}2} = 10.9$ pF. With these dimensions, the coupler is symmetric between the transmitter and receiver.

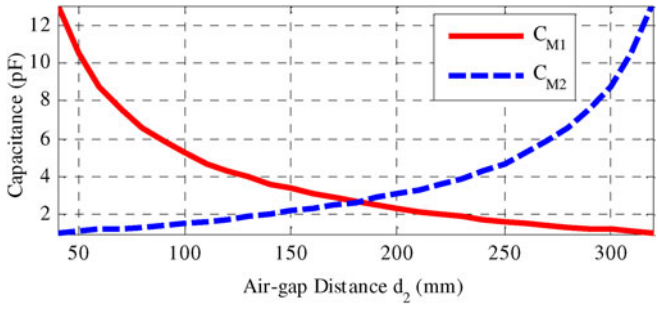

Fig. 6. Maxwell simulation of mutual capacitances at different d_2.

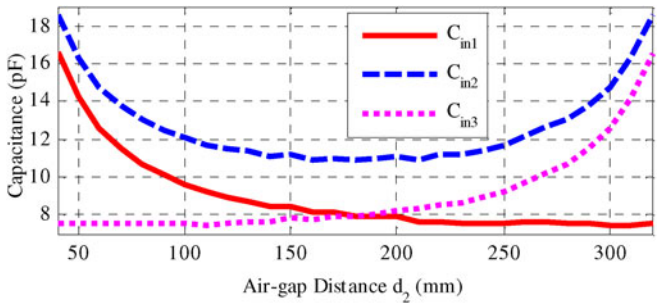

Fig. 7. Maxwell simulation of self-capacitances at different d_2.

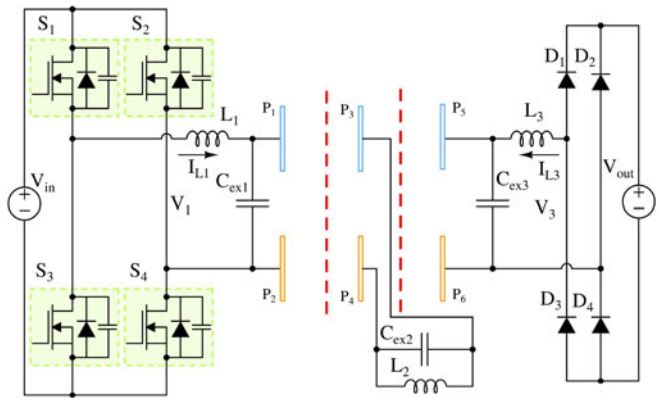

Fig. 8. Circuit topology of an *LC*-compensated electric fields repeater system.

III. Circuit Working Principle

A. Circuit Topology

The circuit topology of an *LC*-compensated electric field repeater system is shown in Fig. 8. At the transmitter side, a full-bridge inverter is used to provide ac excitation. At the receiver side, an uncontrolled rectifier is used to supply dc current to the output battery load. For each pair of plates, an external inductor and an external capacitor are connected to provide resonances.

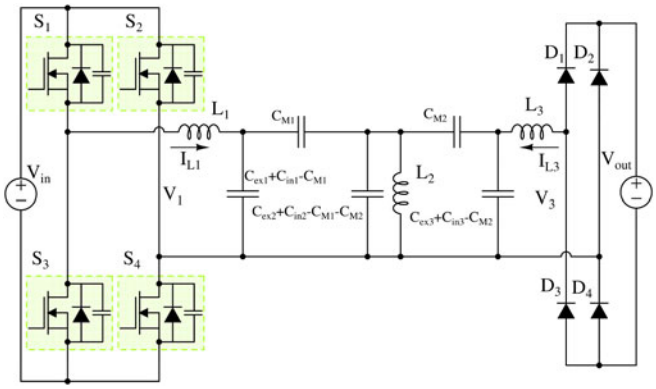

Fig. 9. Equivalent circuit model of the electric fields repeater system.

The capacitive coupler is represented by its equivalent π model in Fig. 5, which results in the equivalent circuit model of the electric field repeater system as shown in Fig. 9. The external capacitors are combined with the self-capacitances of the coupler. The equivalent resonant capacitors are defined as

$$\begin{cases} C_1 = C_{\mathrm{ex1}} + C_{\mathrm{in1}} \\ C_2 = C_{\mathrm{ex2}} + C_{\mathrm{in2}} \\ C_3 = C_{\mathrm{ex3}} + C_{\mathrm{in3}} \end{cases}. \tag{2}$$

B. Working Principle

The fundamental harmonics approximation (FHA) can be used to analyze the circuit working principle, which is shown in Fig. 10. The input and output square-wave voltages are represented by two sinusoidal sources, and the high-order harmonics components are neglected. To simplify the analysis, the power losses in the circuit components are also neglected, which results in the assumption $P_{\mathrm{in}} = P_{\mathrm{out}}$. The simplified circuit topology is shown in Fig. 10(a).

Fig. 10(b) shows the resonant circuit excited by the input soure V_1. The system parameters can be designed to achieve the desired resonance highlighted in Fig. 10(b). The input current flowing through L_1 is zero. If the resonant frequency is designed to be ω_{c}, the relationship between the circuit parameters can be expressed as

$$L_3 \cdot \left(C_3 - \frac{C_{M2}^2}{C_2 - \frac{1}{\omega_c^2 L_2} - \frac{C_{M1}^2}{C_1}} \right) = \frac{1}{\omega_c^2}. \tag{3}$$

This can be further rewritten as

$$C_3 - \frac{1}{\omega_c^2 L_3} = \frac{C_{M2}^2}{C_2 - \frac{1}{\omega_c^2 L_2} - \frac{C_{M1}^2}{C_1}}. \tag{4}$$

In Fig. 10(b), the voltage on L_2 is expressed as

$$V_{L2} = \frac{C_1}{C_{M1}} \cdot V_1. \tag{5}$$

The voltage on L_3 is expressed as

$$V_{L3} = \frac{C_{M2}}{C_3 - \frac{1}{\omega_c^2 L_3}} \cdot V_{L2}. \tag{6}$$

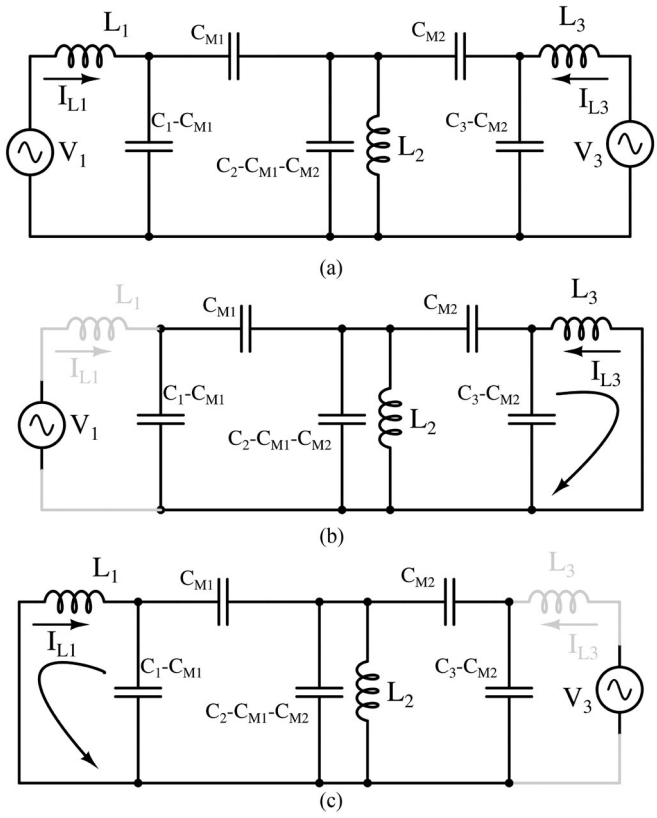

Fig. 10. Fundamental harmonics approximation (FHA) of an *LC*-Compensated electric fields repeater system. (a) Simplified resonant circuit model. (b) Components excited by input source. (c) Components excited by output source.

Then, the current I_{L3} flowing through L_3 is expressed as

$$I_{L3} = -\frac{C_1}{C_{M1}} \cdot \frac{C_{M2}}{C_3 - \frac{1}{\omega_c^2 L_3}} \cdot \frac{1}{j\omega_c L_3} \cdot V_1. \tag{7}$$

Considering the resonance in (4), I_{L3} is further rewritten as

$$I_{L3} = \frac{j\omega_c C_1 C_2 C_3}{C_{M1} C_{M2}} \cdot \left(1 - \frac{1}{\omega_c^2 L_2 C_2} - \frac{C_{M1}^2}{C_1 C_2} - \frac{C_{M2}^2}{C_2 C_3} \right) \cdot V_1. \tag{8}$$

Fig. 10(c) shows the resonant circuit excited by the output source V_2. Similar to the previous condition, the parameters are designed to achieve the highlighted resonance in Fig. 10(c). The output current flowing through L_3 is zero. The parameter relationship is expressed as

$$L_1 \cdot \left(C_1 - \frac{C_{M1}^2}{C_2 - \frac{1}{\omega_c^2 L_2} - \frac{C_{M2}^2}{C_3}} \right) = \frac{1}{\omega_c^2}. \tag{9}$$

It is further rewritten as

$$C_1 - \frac{1}{\omega_c^2 L_1} = \frac{C_{M1}^2}{C_2 - \frac{1}{\omega_c^2 L_2} - \frac{C_{M2}^2}{C_3}}. \tag{10}$$

In Fig. 10(c), the voltage on L_2 is expressed as

$$V_{L2} = \frac{C_3}{C_{M2}} \cdot V_3. \tag{11}$$

The voltage on L_1 is expressed as

$$V_{L1} = \frac{C_{M1}}{C_1 - \frac{1}{\omega_c^2 L_1}} \cdot V_{L2}. \tag{12}$$

Then, the current I_{L1} flowing through L_1 is expressed as

$$I_{L1} = -\frac{C_{M1}}{C_1 - \frac{1}{\omega_c^2 L_1}} \cdot \frac{C_3}{C_{M2}} \cdot \frac{1}{j\omega_c L_1} \cdot V_3. \tag{13}$$

Considering the resonance in (10), I_{L1} is further rewritten as

$$I_{L1} = \frac{j\omega_c C_1 C_2 C_3}{C_{M1} C_{M2}} \cdot \left(1 - \frac{1}{\omega_c^2 L_2 C_2} - \frac{C_{M1}^2}{C_1 C_2} - \frac{C_{M2}^2}{C_2 C_3}\right) \cdot V_3. \tag{14}$$

Since an uncontrolled rectifier is used at the secondary side, V_3 is in phase with $(-I_{L3})$. The current in (8) shows that I_{L3} is 90° leading V_1, and (14) shows I_{L1} is 90° leading V_3. Then, V_1 is also in phase with I_{L1}. Therefore, the input and output power P_{in} and P_{out} are calculated as

$$P_{\text{in}} = P_{\text{out}} = \frac{\omega_c C_1 C_2 C_3}{C_{M1} C_{M2}} \cdot \left(1 - \frac{1}{\omega_c^2 L_2 C_2} - \frac{C_{M1}^2}{C_1 C_2} - \frac{C_{M2}^2}{C_2 C_3}\right) \cdot |V_1| \cdot |V_3|. \tag{15}$$

This shows that the input power is equal to the output power, which agrees with the previous assumption of neglecting the power loss in components.

In this repeater system, the capacitive coupling coefficient k_{C1} and k_{C2} are defined as

$$k_{C1} = \frac{C_{M1}}{\sqrt{C_1 \cdot C_2}},\ k_{C2} = \frac{C_{M2}}{\sqrt{C_2 \cdot C_3}}. \tag{16}$$

In a symmetric system, all the metal plates are designed to be identical. The repeater is placed in the middle of the transmitter and receiver, and C_M is defined as $C_M = C_{M1} = C_{M2}$. The circuit parameters are also designed to be symmetric, which satisfy $L_1 = L_3$ and $C_1 = C_3$, resulting $k_C = k_{C1} = k_{C2}$.

Then, the resonances in (4) and (10) can be simplified as

$$C_1 - \frac{1}{\omega_c^2 L_1} = C_3 - \frac{1}{\omega_c^2 L_3} = \frac{C_M^2}{C_2 - \frac{1}{\omega_c^2 L_2} - \frac{C_M^2}{C_3}} = \frac{C_M^2}{C_2 - \frac{1}{\omega_c^2 L_2} - \frac{C_M^2}{C_1}}. \tag{17}$$

In a symmetric system, the parameters can be designed as

$$\begin{cases} C_M = C_1 - \frac{1}{\omega_c^2 L_1} = C_3 - \frac{1}{\omega_c^2 L_3} \\ C_M = C_2 - \frac{1}{\omega_c^2 L_2} - \frac{C_M^2}{C_1} \end{cases}. \tag{18}$$

By substituting (18) into (15), the system power is simplified as

$$P_{\text{out}} = \frac{\omega_c C_1 \cdot (C_1 - C_M)}{C_M} \cdot |V_1| \cdot |V_3|. \tag{19}$$

Usually, the capacitances can be designed to satisfy $C_1 \approx C_2$ and $C_1 \gg C_M$. Then, (20) can be further simplified as

$$P_{\text{out}} \approx \frac{\omega_c C_M}{k_C^2} \cdot |V_1| \cdot |V_3|. \tag{20}$$

TABLE I
SYSTEM SPECIFICATIONS AND CIRCUIT PARAMETERS

Parameter	Design Value	Parameter	Design Value
V_{in}	60 V	V_{out}	60 V
l_1	300 mm	d_1	150 mm
d_2	180 mm	d_3	180 mm
$C_{\text{in}1}$ ($C_{\text{in}3}$)	8.1 pF	$C_{\text{in}3}$	10.9 pF
C_{M1} (C_{M2})	2.8 pF	$C_{\text{ex}1}$ ($C_{\text{ex}2}$, $C_{\text{ex}3}$)	120 pF
C_1 (C_3)	128.1 pF	C_2	130.9 pF
L_1 (L_3)	89.8 μH	L_2	87.5 μH
k_C	2.19%	f_{sw}	1.5 MHz

IV. 150 W INPUT POWER SYSTEM

In this section, a 150 W input power CPT system with an electric field repeater is designed and simulated. The system specifications and parameters are shown in Table I. The dimensions and capacitances of the capacitive coupler are obtained from the coupler design in Section II, and the remaining circuit parameters are obtained from the analytical calculation in Section III.

In this design, the parameters are designed to be symmetric. The input and output dc voltages V_{in} and V_{out} are set to be 60 V, and the switching frequency f_{sw} is set to be 1.5 MHz. The plate side length is 300 mm, the air-gap distance is 180 mm, and the total transfer distance is 360 mm, resulting in a coupling capacitance C_M of 2.8 pF. In a symmetric system, $C_1 = C_3$, $L_1 = L_3$, and $k_C = k_{C1} = k_{C2}$. According to the system power in (19), C_1 can be calculated. Then, considering the film capacitors available in the lab, the external capacitances $C_{\text{ex}1}$, $C_{\text{ex}2}$, and $C_{\text{ex}3}$ are selected to be 120 pF, and the capacitive coupling coefficient k_C is calculated to be 2.19%. Then, according to the resonances in (18), the inductances L_1, L_2, and L_3 are determined.

Based on the circuit parameters in Table I, LTspice is used to simulate the circuit performance of the designed CPT system. For simplicity, the power losses of circuit components are not considered in the simulation. The system power is simulated to be 150 W, which agrees with the calculation by the power equation (19) and validates the circuit analysis in Section III.

Fig. 11 shows the simulated waveforms of the input and output voltage and current. Considering the direction of the current I_{L3} in Fig. 8, the output current is defined to be $(-I_{L3})$. This indicates that the voltage and current are in phase with each other at both the input and output sides. Moreover, the input voltage V_1 is leading the output voltage V_3 by 90°, which also validates the circuit analysis in Section III.

V. EXPERIMENTS

A. Experimental Setup

Using the parameters in Table I, a prototype of the electric field repeater system is constructed as shown in Fig. 12. Six identical aluminum plates are used to form the capacitive coupler with a repeater. The thickness of the aluminum plates is 2 mm, and the plates are installed on fixtures made from wood. The repeater plates are placed between the transmitter and

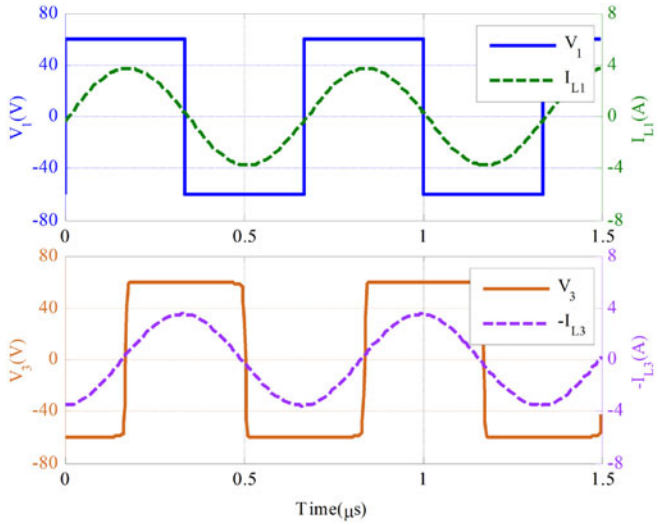

Fig. 11. LTspice-simulated input and output voltage and current waveforms.

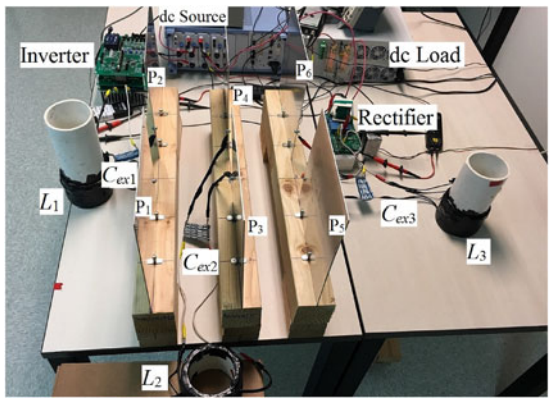

Fig. 12. Experimental prototype of the electric fields repeater system.

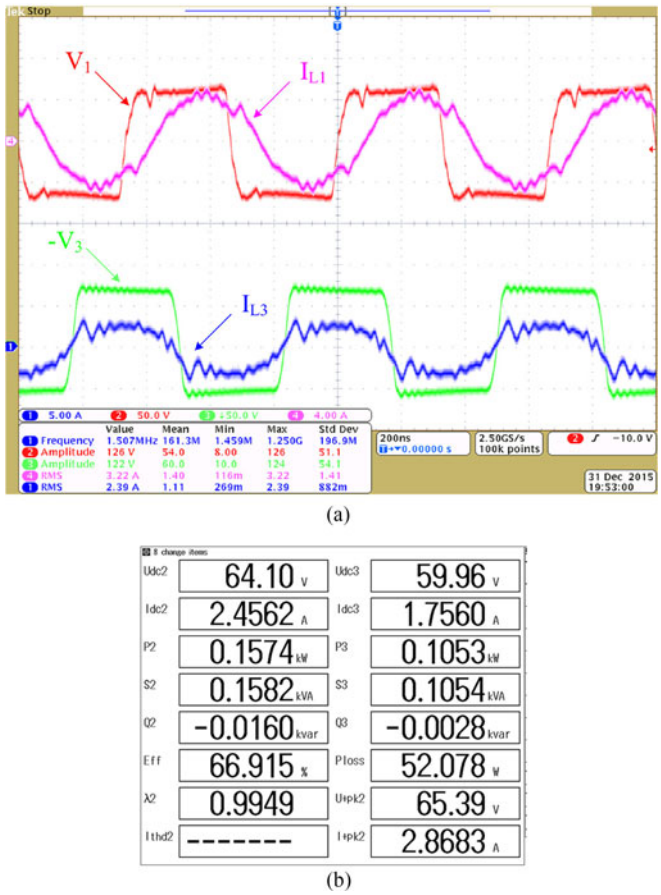

Fig. 13. Experimental results of the electric fields repeater system. (a) Waveforms of input and output voltages and currents. Ch 1(blue): output current I_{L3}; Ch 2 (red): input voltage V_1; Ch 3 (green): inversed output voltage ($-V_3$); Ch 4 (pink): input current I_{L1}. (b) Output power and efficiency.

receiver. The relative position between the plates is adjustable. The parasitic capacitances between the plates and nearby metal can affect the resonances in the circuit. Therefore, the ambient area around the plates is kept clear to eliminate these potential influences. Further research in [25] shows that two shielding plates can help to reduce the interaction between the plates and the nearby metals. In future research, it is a good direction to investigate the parasitic capacitances and their influence on the circuit.

External inductors and capacitors are connected with the plates to provide resonances. In Fig. 12, the inductors are placed far from each other to avoid any inductive coupling between them, and so there are only capacitive couplings in this prototype. The inductors are made from 2175-strand AWG 46 Litz-wire to reduce the conduction losses due to the skin effect in the wires. Also, the inductors have air cores to eliminate the magnetic losses. High-frequency film capacitors from KEMET with a low dissipation factor are used as the external capacitors.

At the input side, a full-bridge inverter with silicon carbide (SiC) MOSFETs (C2M0080120 D) provides ac excitation. A digital controller TMS320 F28335 is used to generate pulse-width modulation (PWM) signals to drive the MOSFETs in the inverter. There is a dead time between the PWM signals, which relates to the soft switching of MOSFETs [26]. The parasitic capacitances of the MOSFETs are charged and discharged during the dead time. In this 1.5 MHz system, the dead time is designed to be 40 ns to realize soft switching of the MOSFETs. At the output side, SiC diodes (IDW30 G65 C) are used in the rectifier, and an electronic dc load is used to emulate a battery load.

B. Experimental Results

In the experiments, all the inductors and capacitors are tuned to the parameter values in Table I. The simulation results in Fig. 11 show that the input voltage V_1 and current I_{L1} are in phase. However, considering the soft switching of MOSFETs in a practical full-bridge inverter, I_{L1} should be slightly lagging V_1 to achieve zero-voltage-switching (ZVS) of the MOSFETs [26]. In this design, the inductor L_1 is increased by 2% to 91.5 μH to achieve ZVS. With these parameters, the experimental results are shown in Fig. 13.

Fig. 13(a) provides the experimental waveforms of the input and output voltages and currents. The input voltage V_1 is measured by Channel 2, and the input current I_{L1} is measured by Channel 4. It shows that I_{L1} is slightly lagging input voltage V_1, which helps to achieve the ZVS condition for the MOS-

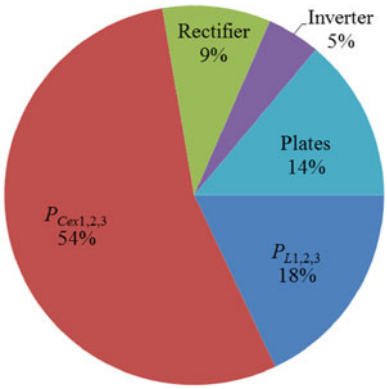

Fig. 14. Estimated power loss distribution among the circuit components.

FETs. The output voltage V_3 is measured by Channel 3, and the measurement signal is inversed in the oscilloscope, resulting in $(-V_3)$ shown in Fig. 13(a). The output current I_{L3} is measured by Channel 1 and the noise in the signal is caused by the low bandwidth of the current probe. In future experiments, the measurement noise can be reduced by better probes. The measurements of signals are also labeled in Fig. 13(a). It shows that $(-V_3)$ is in phase with $-I_{L3}$, and $(-V_3)$ is leading V_1 by 90°, which is consistent with the simulated waveforms in Fig. 11.

In Fig. 13(b), the system input power is 157.4 W and the output power is 105.3 W, which results in a power loss of 52.1 W and a dc–dc efficiency of 66.9% from the dc source to the dc load.

Fig. 14 provides the estimated power loss distribution among circuit components. The calculation of power loss can follow the steps in [7]. The parasitic resistances of the circuit components, including inductors, capacitors, and MOSFETs, can be obtained from their datasheets. The forward voltage of the diodes in the rectifier can also be acquired from the datasheet. Using the simulated currents flowing through the components, their power loss is therefore estimated. Since the ZVS condition is realized for MOSFETs, switching loss can be neglected. The experimental total loss is 52.1 W in Fig. 13(b), and the remaining loss is assumed to be in the metal plates. In future research, the loss in the plates will be modeled and verified using finite element analysis method.

Similar to an IPT system [27], Lu *et al*. in [28] show that the CPT system efficiency also relates to the capacitive coupling coefficient and components' quality facotrs. In this long-distance CPT system, the mutual capacitance is only 2.8 pF and the capacitive coupling coefficient is 2.19%, and so the system efficiency is relative low.

According to the definition of the coupling coefficient in (16), either increasing the mutual capacitance or decreasing the self-capacitances can help to increase the coupling coefficient. In this design, reducing the transfer distance and increasing the plate size can help to increase the mutual capacitance. According to (2), the external capacitances can be reduced to reduce the self-capacitances. However, according to the resonance relationship in (18), this requires to increasing the switching frequency ω_c or the compensation inductances. Considering the limitation of ω_c,

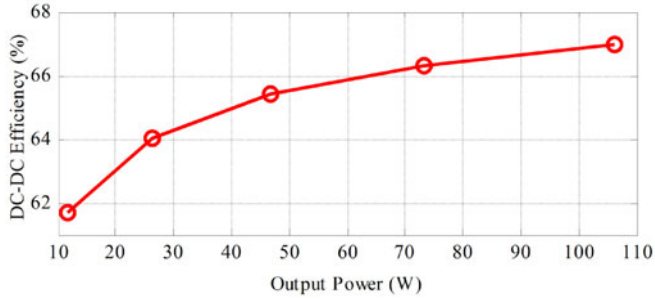

Fig. 15. Experimental dc–dc efficiency at different output power.

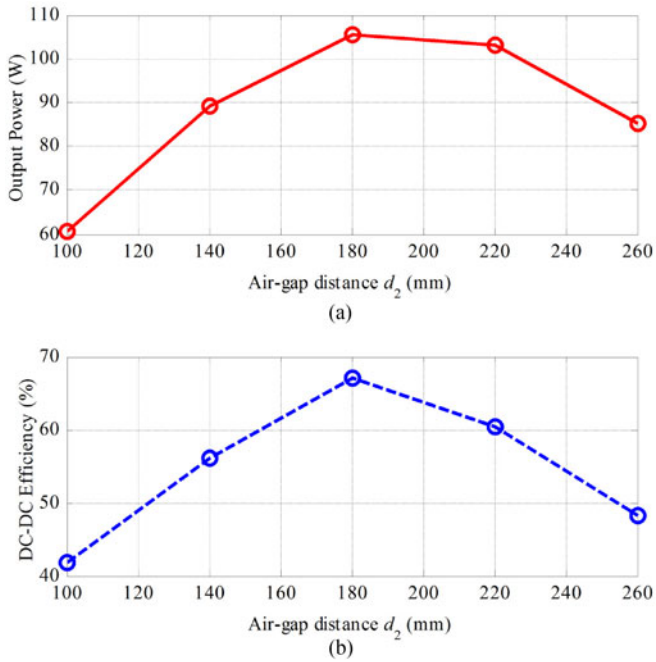

Fig. 16. Experimental output power and efficiency at different d_2. (a) Output power and (b) dc–dc efficiency.

the plate size, and the inductor size, future designs will include all these tradeoffs.

The system dc–dc efficiency was measured at different power level, as shown in Fig. 15. This indicates that the system efficiency increases with output power, and it is getting saturated when the output power is high. After the output power reaches 10 W, the system maintains an efficiency higher than 62%. According to [28], the system efficiency can be improved by increasing the capacitive coupling coefficient and the components' quality factor. For example, better film capacitors with lower dissipation factor can be used as the compensation capacitors.

In a practical applications, the relative position between the repeater and the transmitter can change, which means the air-gap distance d_2 varies. The corresponding system power and efficiency are measured as shown in Fig. 16.

Fig. 16 shows that the middle position is the best location, because the resonances in the circuit, as shown in (4) and (10), are satisfied. When d_2 is reduced to be smaller than 180 mm, the soft-switching condition of MOSFETs cannot be

realized, and so the system power and efficiency decreases. When d_2 increases to be larger than 180 mm, the soft-switching condition is still achieved. However, the reactive power significantly increases, which also reduces the output power and efficiency. Therefore, the prototype achieves maximum output power and efficiency when the repeater is placed in the middle of the transmitter and receiver. In future research, the influence of position variation on system performance will be studied, and the analytical formulation will be provided.

C. Discussion: Comparisons With Nonrepeater Systems

Lu *et al*. in [28] introduces a 180 mm distance *LC*-compensated CPT system without any repeater. Compared with the repeater system in this paper, they have the same geometry of transmitter and receiver plates, the same compensation capacitors, similar compensation inductors, and similar input and output voltages. However, the transfer distance in [28] is only 180 mm, which is half of this repeater system. Experiments show that the power level of these two systems is similar and the 180 mm nonrepeater system can transfer 109.3 W power with a dc–dc efficiency of 74.7%. Therefore, compared to a 180 mm nonrepeater system, one can conclude that a repeater system can double the transfer distance without affecting the system power, but the dc–dc efficiency drops by approximately 7.8%.

A 360 mm distance *LC*-compensated nonrepeater system is constructed as another comparison, in which the repeater is removed and the distance between the transmitter and receiver remains at 360 mm. Compared with the repeater system in this paper, they also have the same input and output votlages and the same compensation components. Since the transfer distance is 360 mm, both the mutual capacitance C_M and the coupling coefficient decreases. According to [28], the power of an *LC*-compensated system is inversely proportional to C_M, so the system power is increased. However, the system efficiency is decreased because of lower coupling coefficient. Experiments are conducted to validate the analysis. At the same input and output votlages, experiments show that the 360 mm nonrepeater system achieves 305.2 W input power and 168.0 W output power with a dc–dc efficiency of 55.0%. Therefore, compared with a 360 mm nonrepeater system, one can conclude that a repeater system can increase the dc–dc efficiency by approximately 11.9%, but the system power is reduced.

A general conclusion can be summarized for the *LC*-compensated repeater system. Compared to a short-distance nonrepeater system, the repeater system can increase the transfer distance at the expense of reduced efficiency; compared to a long-distance nonrepeater system, the repeater system can increase the system efficiency at the expense of reduced power.

In future research, different compensation topologies, such as *LCLC* circuit, will be applied to the repeater system to increase the system power and improve its efficiency, as indicated in [28].

VI. Conclusion

This paper proposes an electric field repeater to extend the transfer distance of the CPT system. The circuit model of the capacitive coupler is proposed, with which the FHA is used to analyze the circuit working principle. A 150 W input power prototype is designed and implemented. The distance between the transmitter and receiver is 360 mm, and the repeater is placed in the middle of them. Experimental results show that the system dc–dc efficiency reaches 66.9%. In future research, there are several interesting directions to investigate, such as the influence of parasitic capacitances with nearby metals, the accurate modeling of plate loss, the improvement of system efficiency, the analytical formulation of the influences of repeater position variation, and the compensation circuit topologies in a repeater system.

References

[1] S. H. Lee, B. S. Lee, and J. H. Lee, "A new design methodology for a 300-kW, low flux density, large air gap, online wireless power transfer system," *IEEE Trans. Ind. Appl.* vol. 52, no. 5, pp. 4234–4242, Sep./Oct. 2016.

[2] M. Etemadrezaei and S. M. Lukic, "Multilayer tubular conductor for high Q-Factor wireless power transfer system resonators," *IEEE Trans. Ind. Appl.* vol. 52, no. 5, pp. 4170–4178, Sep./Oct. 2016.

[3] Y. Zhang, Z. Zhao, and K. Chen, "Frequency-splitting analysis of four-coil resonant wireless power transfer," *IEEE Trans. Ind. Appl.* vol. 50, no. 4, pp. 2436–2445, Jul./Aug. 2014.

[4] S. R. Cove and M. Ordonez, "Wireless-power-transfer planar spiral winding design applying track width ratio," *IEEE Trans. Ind. Appl.* vol. 51, no. 3, pp. 2423–2433, May/Jun. 2015.

[5] A. Abdolkhani, A. P. Hu, G. A. Covic, and M. Moridnejad, "Through-hole contactless slipring system based on rotating magnetic field for rotary applications," *IEEE Trans. Ind. Appl.* vol. 50, no. 6, pp. 3466–3655, Nov./Dec. 2014.

[6] C. Park, S. Lee, G. H. Cho, S. Y. Choi, and C. T. Rim, "Two-dimensional inductive power transfer system for mobile robots using evenly displaced multiple pickups," *IEEE Trans. Ind. Appl.* vol. 50, no. 1, pp. 558–565, Jan./Feb. 2014.

[7] F. Lu, H. Zhang, H. Hofmann, and C. Mi, "A high efficiency 3.3 kW Loosely-Coupled wireless power transfer system without magnetic material," in *Proc. IEEE Energy Convers. Cong. Expo.*, 2015, pp. 2282–2286.

[8] J. Deng, F. Lu, S. Li, T. Nguyen, and C. Mi, "Development of a high efficiency primary side controlled 7kW wireless power charger," in *Proc. IEEE Int. Elect. Veh. Conf.*, 2014, pp. 1–6.

[9] L. Huang, A. P. Hu, and A. Swain, "A resonant compensation method for improving the performance of capacitively coupled power transfer," in *Proc. IEEE Energy Convers. Cong. Expo.*, 2014, pp. 870–875.

[10] J. Dai and D. Ludois, "A survey of wireless power transfer and a critical comparison of inductive and capacitive coupling for small gap applications," *IEEE Trans. Power Electron.*, vol. 30, no. 11, pp. 6017–6029, Nov. 2015.

[11] J. Dai and D. Ludois, "Wireless electric vehicle charging via capacitive power transfer through a conformal bumper," *IEEE J. Emerg. Sel. Topics Power Electron.*, vol. 4, no. 3, pp. 1015–1025, Sep. 2016.

[12] D. C. Ludois, M. J. Erickson, and J. K. Reed, "Aerodynamic fluid bearings for translational and rotating capacitors in noncontact capacitive power transfer systems," *IEEE Trans. Ind. Appl.*, vol. 50, no. 2, pp. 1025–1033, Mar./Apr. 2014.

[13] L. Huang, A. P. Hu, A. Swain, and X. Dai, "Comparison of two high frequency converters for capacitive power transfer," in *Proc. IEEE Energy Convers. Cong. Expo.*, 2014, pp. 5437–5443.

[14] S. H. Lee and R. D. Lorenz, "Development and validation of model for 95%-efficiency 220-W wireless power transfer over a 30-cm air gap," *IEEE Trans. Ind. Appl.*, vol. 47, no. 6, pp. 2495–2504, Nov./Dec. 2011.

[15] S. Aldhaher, P. C. Luk, A. Bati, and J. F. Whidborne, "Wireless power transfer using class E inverter with saturable DC-feed inductor," *IEEE Trans. Ind. Appl.*, vol. 50, no. 4, pp. 2710–2718, Jul./Aug. 2014.

[16] F. Lu, H. Zhang, H. Hofmann, and C. Mi, "A double-sided LCLC-compensated capacitive power transfer system for electric vehicle charging," *IEEE Trans. Power Electron.*, vol. 30, no. 11, pp. 6011–6014, Nov. 2015.

[17] F. Lu, H. Zhang, H. Hofmann, and C. Mi, "A CLLC-compensated high power and large air-gap capacitive power transfer system for electric ve-

hicle charging application," in *Proc. IEEE Appl. Power Electron. Conf.*, 2016, pp. 1721–1725.
[18] H. Zhang, F. Lu, H. Hofmann, and C. Mi, "A 4-Plate compact capacitive coupler design and LCL-compensated topology for capacitive power transfer in electric vehicle charging applications," *IEEE Trans. Power Electron.*, vol. 31, no. 12, pp. 8541–8551, 2016.
[19] F. Lu, H. Zhang, H. Hofmann, and C. Mi, "An inductive and capacitive combined wireless power transfer system with LC-Compensated topology," *IEEE Trans. Power Electron.*, vol. 31, no. 12, pp. 8471–8482, Dec. 2016.
[20] C. K. Lee, W. X. Zhong, and S. Y. Hui, "Recent progress in Mid-Range wireless power transfer," in *Proc. IEEE Energy Convers. Cong. Expo.*, 2012, pp. 3819–3824.
[21] W. X. Zhong, C. K. Lee, and S. Y. Hui, "General analysis on the use of Tesla's resonators in domino forms for wireless power transfer," *IEEE Trans. Power Electron.*, vol. 60, no. 1, pp. 261–270, Jan. 2013.
[22] K. E. Koh, T. C. Beh, T. Imura, and Y. Hori, "Impedance matching and power division using impedance inverter for wireless power transfer via magnetic resonant coupling," *IEEE Trans. Ind. Appl.* vol. 50, no. 3, pp. 2061–2070, May/Jun. 2014.
[23] H. Zhang, F. Lu, H. Hofmann, W. Liu, and C. Mi, "An LC Compensated electric field repeater for long distance capacitive power transfer," in *Proc. IEEE Energy Convers. Cong. Expo.*, 2016, pp. 1–5.
[24] M. kusunoki, D. Obara, and M. Masuda, "Wireless power transfer via electric field resonance coupling," in *Proc. IEEE Asia-Pacific Microw. Conf.*, 2014, pp. 1360–1362.
[25] H. Zhang, F. Lu, H. Hofmann, and C. Mi, "A six-plate capacitive coupler to reduce electric field emission in large air-gap capacitive power transfer," *IEEE Trans. Power Electron.*, to be published. doi: 10.1109/TPEL.2017.
[26] S. Li, W. Li, J. Deng, T. D. Nguyen, and C. Mi, "A Double-Sided LCC compensation network and its tuning method for wireless power transfer," *IEEE Trans. Veh. Tech.*, vol. 64, no. 6, pp. 2261–2273, Jun. 2015.
[27] S. Li and C. Mi, "Wireless power transfer for electric vehicle applications," *IEEE J. Emerg. Sel. Topics Power Electron.*, vol. 3, no. 1, pp. 4–17, Mar. 2015.
[28] F. Lu, H. Zhang, H. Hofmann, and C. Mi, "An double-sided LC compensation circuit for loosely-coupled capacitive power transfer," *IEEE Trans. Power Electron.*, to be published. doi: 10.1109/TPEL.2017.2674688.

Hua Zhang (S'14) received the B.S. and M.S. degrees in electrical engineering from Northwestern Polytechnical University, Xi'an, China, in 2011 and 2014, respectively, and where she is currently working toward the Ph.D. degree in electrical engineering.

From September 2014 to August 2015, she was a joint Ph.D. student founded by the China Scholarship Council with the University of Michigan, Dearborn, MI, USA. From September 2015, she joined San Diego State University, San Diego, CA, USA. Her research interests include the coupler design of high-power inductive power transfer and capacitive power transfer systems.

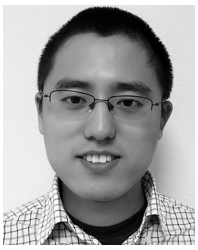

Fei Lu (S'12) received the B.S. and M.S. degrees in electrical engineering from the Harbin Institute of Technology, Harbin, China, in 2010 and 2012, respectively, and the Ph.D. degree in electrical engineering from the University of Michigan, Ann Arbor, MI, USA, in 2017.

He is currently working as a Postdoctoral Researcher with San Diego State University, San Diego, CA, USA. His research interests include wireless power transfer for the application of electric vehicle charging. He is working on the high power and high-efficiency capacitive power transfer through an air-gap distance up to 100's of millimeters. He is also working on the application of wide band-gap devices on wireless power transfer system to increase the system frequency.

Heath Hofmann (M'89–SM'15) received the B.S. degree in electrical engineering from the University of Texas at Austin, Austin, TX, USA, in 1992, and the M.S. and Ph.D. degrees in electrical engineering and computer science from the University of California, Berkeley, CA, USA, in 1997 and 1998, respectively.

He is currently an Associate Professor with the University of Michigan, Ann Arbor, MI, USA. His research interests include the design, analysis, and control of electromechanical systems, and power electronics.

Weiguo Liu (SM'07) received the B.S. degree in electrical machines engineering from the Huazhong University of Science and Technology, Wuhan, China, in 1982, and the M.S. degree in electrical engineering and the Ph.D. degree in control theory and control engineering from Northwestern Polytechnical University, Xi'an, China, in 1988 and 1999, respectively.

He is a Professor with the Department of Electrical Engineering, Northwestern Polytechnical University, and a Guest Professor with the University of Federal Defense, Munich, Germany. He is the Director of the Institute of Rare Earth Permanent Magnet Electrical Machines and Control Technology, Northwestern Polytechnical University. His research interests include brushless dc machines, PM synchronous machines, dc machines, and induction machines.

Prof. Liu was the Chairman of the Organizing Committee of the 32nd Chinese Control Conference, July 2013, Xi'an.

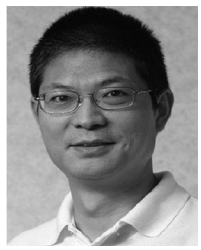

Chunting Chris Mi (S'00–A'01–M'01–SM'03–F'12) received the B.S.E.E. and M.S.E.E. degrees in electrical engineering from Northwestern Polytechnical University, Xi'an, China, and the Ph.D. degree in electrical engineering from the University of Toronto, Toronto, ON, Canada, in 1985, 1988, and 2001, respectively.

He is a Professor and Chair of electrical and computer engineering, and the Director of the Department of Energy (DOE)-funded Graduate Automotive Technology Education (GATE) Center for Electric Drive Transportation with San Diego State University (SDS), San Diego, CA, USA. Prior to joining SDSU, he was at with University of Michigan, Dearborn, MI, USA, from 2001 to 2015. He was the President and the Chief Technical Officer of 1Power Solutions, Inc., Cupertino, CA, from 2008 to 2011. He is the Co-Founder of Gannon Motors and Controls LLC, San Diego, and Mia Motors, Inc. San Diego. His research interests include electric drives, power electronics, electric machines, renewable-energy systems, and electrical and hybrid vehicles. He has conducted extensive research and has published more than 100 journal papers. He has taught tutorials and seminars on the subject of Hybrid Electric Vehicle (HEVs)/Plug-in Hybrid Electric Vehicle (PHEVs) for the Society of Automotive Engineers (SAE), the IEEE, workshops sponsored by the National Science Foundation (NSF), and the National Society of Professional Engineers. He has delivered courses to major automotive Original Equipment Manufacture (OEMs) and suppliers, including GM, Ford, Chrysler, Honda, Hyundai, Tyco Electronics, A&D Technology, Johnson Controls, Quantum Technology, Delphi, and the European Ph.D School. He has offered tutorials in many countries, including the U.S., China, Korea, Singapore, Italy, France, and Mexico. He has published more than 100 articles, and has delivered 30 invited talks and keynote speeches. He has also served as a panelist at major IEEE and SAE conferences.

Dr. Mi received the Distinguished Teaching Award and the Distinguished Research Award from the University of Michigan. He also received the 2007 IEEE Region 4 Outstanding Engineer Award, the IEEE Southeastern Michigan Section Outstanding Professional Award, and the SAE Environmental Excellence in Transportation (E2T) Award.